Nanotechnology

PAPER

Confocal scanning photoluminescence for mapping electron and photon beam-induced microscopic changes in SiN_x during nanopore fabrication

To cite this article: Xiaodong He *et al* 2020 *Nanotechnology* **31** 395202

IOP Publishing Nanotechnology

Nanotechnology **31** (2020) 395202 (11pp) https://doi.org/10.1088/1361-6528/ab9bd4

Confocal scanning photoluminescence for mapping electron and photon beam-induced microscopic changes in SiN_X during nanopore fabrication

Xiaodong He[1,2], Zifan Tang[1], Shengfa Liang[3], Ming Liu[3] and Weihua Guan[1,4,5]

[1] Department of Electrical Engineering, Pennsylvania State University, University Park, PA 16802, United States of America
[2] School of Information Science and Engineering, Lanzhou University, Lanzhou 730000, People's Republic of China
[3] Key Lab of Microelectronic Devices & Integrated Technology, Institute of Microelectronics, Chinese Academy of Sciences, Beijing 100029, People's Republic of China
[4] Department of Biomedical Engineering, Pennsylvania State University, University Park, PA 16802, United States of America
[5] Materials Research Institute, Pennsylvania State University, University Park, PA 16802, United States of America

E-mail: w.guan@psu.edu

Received 19 March 2020, revised 29 May 2020
Accepted for publication 11 June 2020
Published 9 July 2020

Abstract

Focused electron and laser beams have shown the ability to form nanoscale pores in SiN_x membranes. During the fabrication process, areas beyond the final nanopore location will inevitably be exposed to the electron beams or the laser beams due to the need for localization, alignment and focus. It remains unclear how these unintended exposures affect the integrity of the membrane. In this work, we demonstrate the use of confocal scanning photoluminescence (PL) for mapping the microscopic changes in SiN_x nanopores when exposed to electron and laser beams. We developed and validated a model for the quantitative interpretation of the scanned PL result. The model shows that the scanning PL result is insensitive to the nanopore size. Instead, it is dominated by the product of two microscopic material factors: quantum yield profile (i.e. variations in electronic structure) and thickness profile (i.e. thinning of the membrane). We experimentally demonstrated that the electron and laser beams could alter the material electronic structures (i.e. quantum yield) even when no thinning of the membrane occurs. Our results suggest that minimizing the unintended e-beam or laser beam to the SiN_x during the fabrication is crucial if one desires the microscopic integrity of the membrane.

Supplementary material for this article is available online

Keywords: photoluminescence, silicon nitride, nanopore, confocal, scanning

(Some figures may appear in colour only in the online journal)

1. Introduction

Solid-state nanopores have emerged as an increasingly appealing alternative to biological nanopores in translocation studies for analyzing nucleic acids [1–4] and proteins [5, 6]. This is largely attributed to their mechanical and chemically robustness, tunable size, and potential for integration and miniaturization. In general, solid-state nanopores have been formed in synthetic dielectric materials such as SiN_x [7], SiO_2 [8], Al_2O_3 [9], TiO_2 [10], HfO_2 [11], as well as emerging 2D materials

(e.g. graphene [12, 13], MoS_2 [14–17], BN [18, 19], WS_2 [20] and MXenes [21]). Among these thin-film materials, SiN_x is the most thoroughly studied nanopore material, and has traditionally been fabricated by a focused electron beam [22–26] or ion beam [27–29] in vacuum due to their small wavelength. Nevertheless, recent studies have demonstrated that a focused laser beam at a visible wavelength can also be used for forming nanoscale holes in SiN_x materials (this mostly needs to be done in aqueous solutions, with additional electric fields applied, either for monitoring [30, 31] or for electrical stressing [31, 32]). For example, Gilboa *et al* showed that a focused 488 nm laser beam with an intensity of a few tens ofilliwatts could irreversibly etch SiN_x membranes for nanometer-scale pores in 1 M KCl [30]. They also found that the etching process is extremely sensitive to the relative content of Si and N atoms in the SiN_x membrane [31]. Yamazaki *et al* showed that the SiN_x etching rate with similar laser intensity and wavelength was influenced by the chemical components of the electrolyte and suggested that the laser-induced heating effect plays the dominant role [32]. Ying *et al* showed that infrared laser (808 nm)-assisted controlled breakdown [33, 34] can significantly reduce the probability of forming multiple nanopores with the help of laser-induced local heating [35].

It is now clear that both focused electron beams and laser beams could be used for forming nanopores in SiN_x membranes. From the material perspective, the nanopores can be considered as point defects in the SiN_x membranes. In other words, an ideal nanopore fabrication process should aim to create a nanoscale vacancy in the thin film. However, areas beyond the final nanopore spot (nanometer scales) will inevitably be exposed to the electron beams or the laser beams during the fabrication process because of the need for localization, alignment and focus. Although these preparatory exposures often do not produce observable changes in the morphology of SiN_x, it remains unclear whether they will alter the microscopic structure and affect the integrity of the membrane.

Photoluminescence (PL) spectroscopy is a well-established technique to probe the material's microscopic structures. PL in amorphous SiN_x thin films is a well-characterized phenomenon in both air and solutions [10, 36–41]. The background PL emitted from SiN_x was deemed undesirable for optical sensing of the analyte [10, 41] due to the fluorescence interference. The PL of SiN_x is most likely due to the Si dangling bonds (defect states) that promote the recombination of photogenerated carriers. Previous studies have shown that the SiN_x PL spectra shift toward higher energies as the nitride content increases [37, 40]. Scanning PL was previously used for profiling the SiN_x nanopores drilled by a transmission electron microscope (TEM), and it was observed that there was a pronounced reduction in PL emission in the nanopore area [30, 41].

In this work, we demonstrate the use of confocal scanning PL for mapping microscopic changes in SiN_x nanopores exposed to electron and laser beams. A quantitative model was developed to interpret the scanning PL results. Our model revealed that the PL reduction has nothing to do with the nanopore size. The observed PL reduction results from the product of two microscopic factors: variations in quantum yield (i.e. electronic structure) and variations in thickness (i.e. thinning of the membrane) due to the exposure to the radiation beams. We have unambiguously shown that unintended electron and laser beam exposure would significantly change the electronic structures in the SiN_x membrane, even when there is no visible thinning of the membrane. We anticipate that this work will provide experimental insights into beam-based SiN_x nanopore fabrication and characterization.

2. Results and discussion

2.1. Quantitative modeling of confocal scanning PL

Figure 1(a) is a diagram of our custom-built confocal scanning PL setup (see section 4 for details) for profiling the SiN_x nanopores (figures 1(b)–(d)). For any point r on the SiN_x membrane, the number of emitted photons can be described by [42, 43]

$$E(r) = \frac{I_{ex}(r)}{h\nu}\alpha d(r)\,\Phi_F(r) \tag{1}$$

where $I_{ex}(r) = (2P/\pi w_{laser}^2)\exp\left(-2r^2/w_{laser}^2\right)$ is the excitation intensity at point r, in which P is the incident laser power, w_{laser} is the laser spot size (distance from the beam axis where the intensity drops to $1/e^2$ of the maximum value). $h\nu$ is the incident photon energy. α is the absorption coefficient. $d(r)$ and $\Phi_F(r)$ are the thickness and the fluorescence quantum yield at point r on the SiN_x membrane, respectively. Note that the profile of $d(r)$ and $\Phi_F(r)$ can be varied by the exposure to the electron and laser beams through either thinning of the membrane or alteration of the electronic structure, depending on the incident energy.

For the confocal setup, a pinhole was used to achieve maximal background rejection [44]. The transmission function $t_p(r)$ for the pinhole with image radius R can be written as

$$t_p(r) = \begin{cases} 1, & |r| < R \\ 0, & |r| > R. \end{cases} \tag{2}$$

The probability of an emitted photon being transmitted through the pinhole and getting detected is given by the convolution of $t_p(r)$ and the detection function $I_{det}(r)$,

$$c_p(r) = t_p(r) * I_{det}(r) = \int_0^R r'dr' \int_0^{2\pi} \exp\left(-2\frac{r^2 - 2r'r\cos\Phi + r'^2}{w_{det}^2}\right) d\Phi. \tag{3}$$

Note that the half-width at half-maximum (HWHM) of the confocal acceptance function (CAF), which defines the confocal resolution is calculated romy $caf(r) = I_{ex}(r)\,c_p(r)$. The HWHM of the CAF as a function of pinhole size is analyzed in supplementary figure S1 (available at stacks.iop.org/NANO/31/395202/mmedia). It was found that while decreasing the pinhole size can indeed enhance the resolution, the enhancement is saturated when the pinhole diameter is around 25 μm (the size we used in our setup).

When the excitation laser is focused at point r on the membrane, the total number of photons counted per unit time is

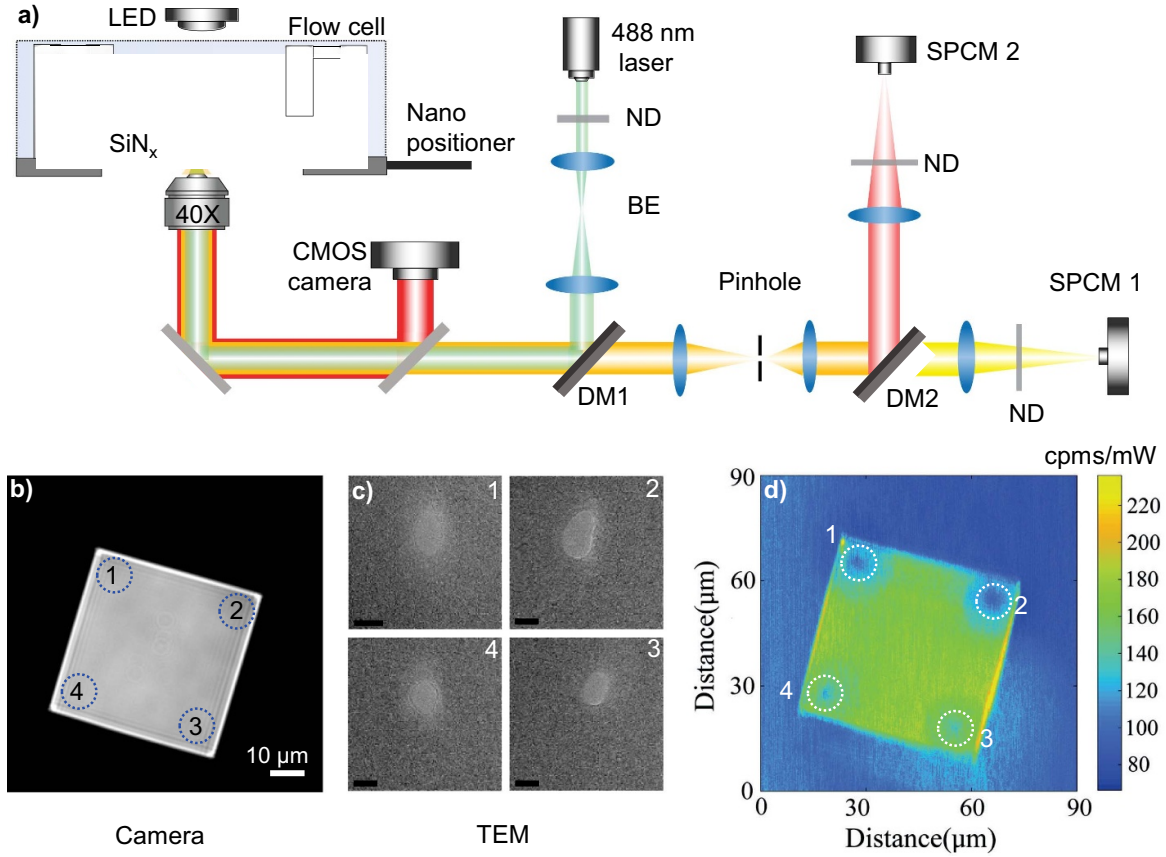

Figure 1. (a) Experimental setup of the confocal scanning PL system. (b) Microscope image of the entire SiN_x membrane ($50 \times 50\ \mu m^2$) in which four nanopores were drilled with a highly focused e-beam near the four corners. (c) TEM images of the as-drilled nanopores; the scale bar for all TEM images is 10 nm. (d) PL map of the SiN_x sample (10 mW, 488 nm excitation, 2 ms photon counter integration time, 300 nm scan step). The counted emission photons were normalized to the integration time and the incident laser power (cpms: counts per millisecond).

given by the *convolution* of $E(r)$ and $c_p(r)$, multiplied by the system collection efficiency η, which is related to the objective, bandpass filters and lens. The noise sources would consist of the Poisson noise, the background signal and the dark counts [42, 43]. Therefore, the total photons counted during a time T (integration time) would be given by

$$S(r') = \underbrace{\eta TE(r) * c_p(r)}_{signal} + \underbrace{\sqrt{\eta TE(r) * c_p(r) + C_b PT + N_d T}}_{noise} \quad (4)$$

in which N_d is the dark count rate and C_b is the background count rate per watt of excitation power. Equation (4) essentially describes the total measured PL as a function of the laser location.

2.2. Interpretation of scanning PL results

With the confocal scanning PL model (equation (4)) and the experimentally determined setup parameters listed in supplementary table S1, we calculated the PL map as a function of various combinations of nanopore size, the material's microscopic profiles (defined as $d(r)\,\Phi_F(r)$) and the excitation laser profiles $I_{ex}(r)$. Figure 2(a) shows the results for a fixed excitation laser spot size (1.2 μm). Each column and row represents a specific nanopore size and microscopic profile, respectively. The first row shows the result with a uniform material profile across the SiN_x membrane (i.e. no variations in the electronic structures and thickness; the only thickness variation is at the nanopore spot). In this case, no clear PL reduction can be observed when the nanopore size varies from 10 nm to 100 nm. This is not surprising since the nanopores, with sizes of tens of nanometers, were below the spatial resolution of the confocal scanning PL (509 nm). This result shows that the contribution of the nanopore itself to the PL reduction is too small to be observed (easily overwhelmed by the noise).

If the nanopore size alone cannot reproduce the experimental observation of the reduced PL [30, 41], the product $d(r)\,\Phi_F(r)$ (i.e. microscopic profiles of the material) must be taken into consideration for interpreting the scanning PL results. For the electron beam, although it is highly focused into a few nanometers in the final drilling process, the preparatory steps such as zooming in during the fabrication can result in exposed areas spreading several microns. For the laser beam, the exposed area is limited by the spot size (~1.2 μm). These exposures can result in possible microscopic variations spread over several microns. The second to the fourth rows in figure 2(a) show the results with various microscopic profiles. As shown, the obtained scanning PL result

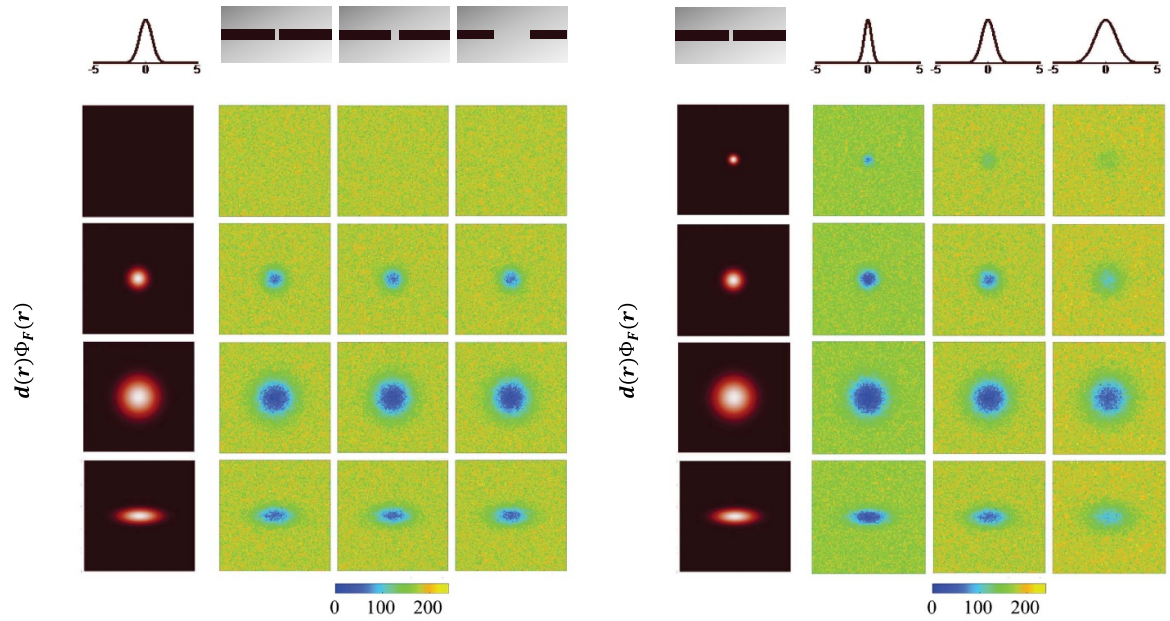

Figure 2. (a) Simulated PL maps for various nanopore sizes *columns* and microscopic profiles of the material (defined as the product of the quantum yield and the thickness: rows). The excitation laser spot size is fixed at 1.2 μm. Note that the material's microscopic profiles from the second to fourth row spread over several microns, much larger than typical nanopore dimensions. The resulting PL map is highly correlated to the microscopic profiles and is independent of the nanopore size. (b) Simulated PL maps for various laser spot sizes *columns* and microscopic profiles of the material *rows*. The nanopore size is fixed at 10 nm. A tightly focused laser can improve the resolution of the scanned PL. All of the simulations were carried out at laser power 1 mW, integration time 2 ms and scanning step 100 nm. The thickness and the quantum yield in the intact membrane are 30 nm and 1%, respectively.

is strongly correlated to the microscopic profile and is independent of the nanopore size. These results indicate that the spatial distribution of the scanning PL map is a measurement of the microscopic profile and has nothing to do with the nanopore size due to the fact the most nanopores (as point defects) are well below the spatial resolution of the optical setup.

We also studied the impact of the laser spot size on the scanned PL result. Figure 2(b) shows the results for a fixed 10 nm nanopore and various laser spot sizes. Again, the scanned PL result is strongly correlated to the microscopic profile and is weakly dependent on the laser spot size. However, it is clear from the results shown in figure 2(b) that a highly focused laser can indeed improve the resolution of the scanned PL. This suggests that one should always try to get the best focus when performing the scanning PL experiment.

Results in figures 2(a) and (b) clearly show that the scanned PL result is a mapping of the thin membrane material's microscopic profile, rather than the nanopore geometry or size. This explains why Assad *et al* observed a significant PL reduction even when there is no nanopore formed [41]. The microscopic profile is correlated to the material's electronic structure (e.g. compositional variations, defects) as well as its morphology (e.g. thickness variations). Therefore, the scanned PL approach can be a suitable technique for probing the microscopic changes in silicon nitride nanopores exposed to electron and laser beams, independent of the nanopore size.

2.3. Enhancing the SNR of scanning PL

According to equation (4), the PL signal depends on the laser power P and integration time T linearly, while the noise depends on the laser power and integration time as $P^{1/2}$ and $T^{1/2}$. To test whether this is consistent with experiments, we measured a plain 30 nm thick free-standing SiN_x membrane (without any nanopores). Figure 3(a) shows the signal and rms noise of the counted PL value at different laser powers with 2 ms integration time. Each data point results from the 10 measurements. The average value and standard deviation of the PL counts were considered as the signal and noise, respectively. We observed that the signal indeed increases linearly with laser power (P), while the noise increases with the square root with laser power ($P^{1/2}$). Figure 3(b) shows the PL signal and rms noise as a function of photocounter integration time at a constant laser power of 1 mW. Again, the signal and noise showed the expected dependence on T and $T^{1/2}$, respectively. It is noteworthy that the results in figures 3(a) and (b) enabled us to experimentally determine the model parameters for our customized confocal PL setup (supplementary table S1).

The PL signal-to-noise ratio (SNR) depends on the laser power and integration time as $P^{1/2}$ and $T^{1/2}$. As expected, increasing the laser power and integration time is favorable for obtaining the PL map with improved SNR. To verify this, we scanned a 10 $\times$ 10 μm^2 region of the SiN_x membrane with a TEM-drilled nanopore of ~10 nm diameter in the center. Figure 3(c) shows the PL maps at five different laser powers ranging from 100 μW to 5 mW. Note that the obtained PL map is a measurement of the microscopic profile around the nanopore,

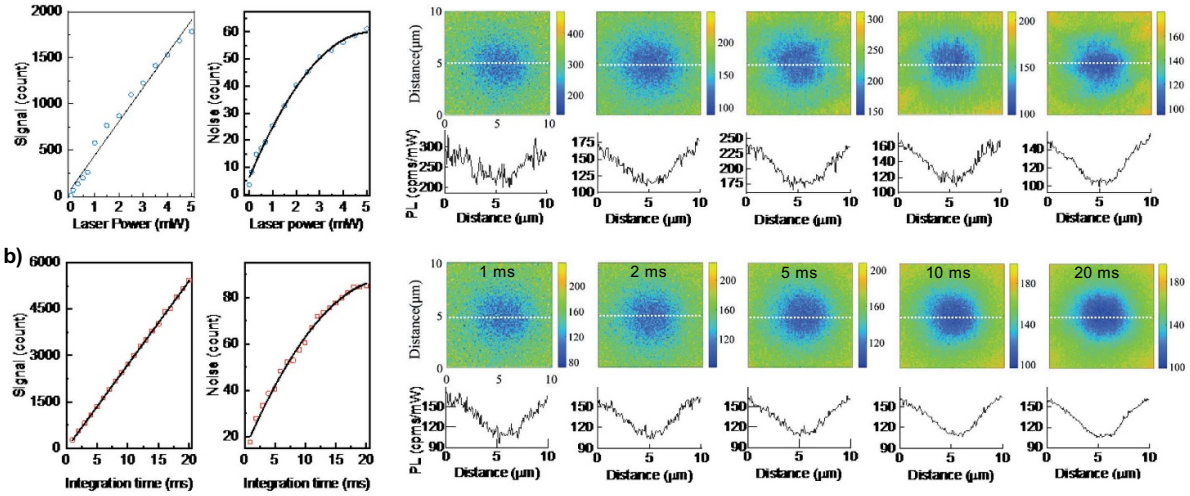

Figure 3. (a) The PL signal and noise from a 30 nm thick SiN_x membrane at different laser powers (2 ms integration time). (b) The PL signal and noise at different integration times (constant 1 mW laser power). The open circles and squares are experimental data. Lines are linear and square-root fitting. Each data point was from 10 measurements. (c) PL maps of a 10 nm nanopore in the center of the SiN_x membrane for various laser powers (2 ms integration time) with the corresponding line profiles. (d) PL maps of the same sample at various integration times (constant 0.5 mW laser power), with the corresponding line profiles plotted underneath.

rather than the nanopore itself. As expected, increasing the laser power indeed improved the SNR of the PL map, which was evident from the corresponding line profile (bottom plots in figure 3(c)). Although higher laser power is preferred for an improved SNR, it is noteworthy that higher power itself can impact (or damage) the sample under test, as we will discuss later. Figure 3(d) shows the PL maps for five different integration times (1–20 ms) at a constant laser power of 0.5 mW, with the corresponding line profile shown underneath. It was clear that increasing the integration time can effectively improve the SNR of the PL mapping, consistent with the model predictions.

2.4. Impact of electron beams on membrane integrity

It was reported that the high-dose electron-beam irradiation at 200 kV (common for TEM nanopore drilling) could cause fast damage to thin-film material with modifications to both the morphology (e.g. thinning of the membrane [45]) and the chemical composition (e.g. oxidized surfaces [46], the formation of bubble-like defects [47], electrostatic charging [48], and the creation of a locally enriched silicon area by preferential depletion of nitrogen atoms [49]). The e-beam radiation-induced modification to the chemical composition would change the local band structure as well as the local quantum yield of SiN_x [40, 50–55].

To investigate the impact of e-beam irradiation on membrane integrity, after drilling the nanopore, we purposefully reduced the TEM magnification to 15k such that the non-drilling e-beam irradiation area is ~14 μm in diameter (figure 4(a)). Figure 4(b) shows the resulting PL map. It was found that the PL reduction area was consistent with the e-beam irradiation area (~14 μm diameter), although the nanopore was only 7 nm in diameter (inset of figure 4(a)). To quantify the relationship between the PL reduction and e-beam dose, we examined six membranes with different irradiation times at 15k magnification (figure 4(c)). Figure 4(d) shows the changes in PL reduction percentage as a function of e-beam irradiation time. The PL reduction percentage was calculated by comparing the average PL intensity in the e-beam exposed area and that in the non-exposed area. The PL reduction shows a nonlinear dependence on the e-beam irradiation time. The PL reduction becomes saturated after 6 min. These observations are in excellent agreement with previous studies [41]. This result suggests that the low-intensity e-beam exposure did not etch the membrane (otherwise PL reduction would vary linearly with time and would decay asymptotically to zero when it is fully etched). The saturation of PL reduction is most likely due to the saturated electron trapping in the irradiation area [48, 55].

During the TEM based nanopore fabrication process, the final nanopore area receives the most energy when the electron beam is highly focused, while areas beyond the final nanopore spot will inevitably be exposed to the electron beams when performing localization, alignment and focus. In an attempt to fabricate a single nanopore in the center of a 50 $\times$ 50 μm^2 free-standing SiN_x membrane (figure 5(a)), we firstly focused the e-beam to the window edges to determine the coordinates before moving to the membrane center, where the nanopore was drilled (figure 5(b)). The PL map of this sample is shown in figure 5(c). While we indeed observed the most pronounced PL reduction around the 20 nm nanopore, the PL map of this sample surprisingly showed a clear trace from the lower right corner to the membrane center that was not reported before. In another attempt to drill three nanopores on the SiN_x membrane (figures 5(d) and (e)), the PL map also showed clear traces that followed the e-beam path during the fabrication (figure 5(f)).

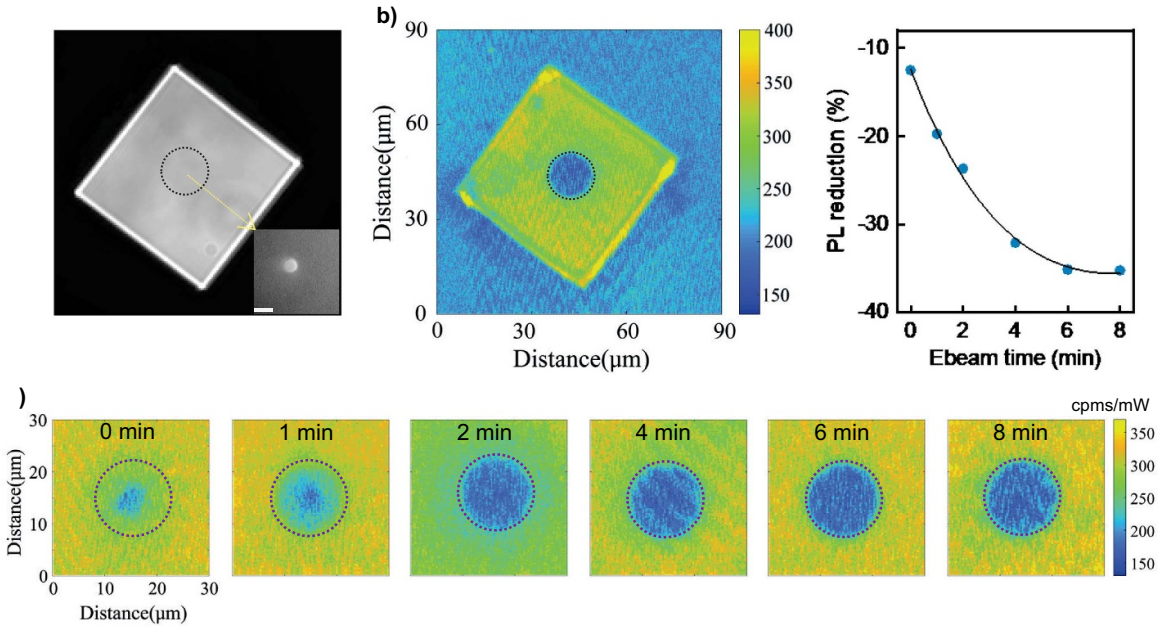

Figure 4. (a) The image of a 50 × 50 μm^2 SiN_x membrane showing a 14 μm diameter area (dashed circles) that was irradiated with the non-etching e-beam (beam current 158 μA). The inset shows the nanopore in the center of this irradiation area (scale bar, 10 nm). (b) The resulting PL map with 8 min e-beam irradiation. (c) PL maps for various e-beam irradiation times (0 min means no additional exposure after drilling the nanopore). (d) The PL reduction percentage as a function of e-beam irradiation time. The solid line is an exponential fit to the experiment data (blue dots). The PL maps were obtained for laser power 1 mW, integration time 2 ms and scanning step 300 nm.

Since there was no observable etching occurring along the path traversed by the e-beam (verified by TEM), the significant PL reduction along the path is mainly contributed by the change in quantum yield (i.e. the e-beam-induced change in electronic structure). The microscopic nature of this change in electronic structure would require further detailed compositional analysis of the local material, which is beyond the scope of this work. Nevertheless, it can be hypothesized that the change in electronic structure of the membrane caused by the e-beam will likely impact the noise performance of nanopore sensors [56–58], which needs to be examined systematically in future studies. Practically, in order to minimize the impact of the e-beam on the membrane integrity during the fabrication, the e-beam should be quickly moved to the desired nanopore location and be turned off immediately after drilling the nanopore.

2.5. *Impact of laser beams on membrane integrity*

While increasing the laser power can help improve the SNR of the PL mapping (figure 3(c)), high laser power itself can result in changing the microstructure and chemical composition of the material. To investigate the impact of the incident laser beams on SiN_x membrane, we sequentially irradiated different locations on a single membrane with a focused 488 nm laser at various laser powers and exposure times in air with humidity ~60% (figure 6(a)). The sample was then examined by the scanned PL method at 1 mW intensity, the result of which is shown in figure 6(b). It was clear that the incident laser alone will induce the reduction in PL, giving enough exposure energy. In general, increasing the laser power and irradiation time will produce a more pronounced reduction in PL.

To understand the nature of this laser-induced PL reduction in the air, the same sample was further characterized by atomic force microscopy (AFM). As shown in figure 6(c), at relatively low laser energy (less than 10 mW for up to 20 min exposure), no significant change in morphology was observed within the resolution of the AFM, although the PL reduction is evident (figure 6(b)). This suggests the PL reduction is likely due to the altered electronic structures at low laser energy. On the other hand, at relatively high laser power (*e.g.* 15 mW for > 10 min exposure), we surprisingly found that the area exposed to the laser was larger (instead of smaller) than the intact area of the membrane. For example, 20 min exposure at 15 mW laser power will result in about 8 nm greater exposed area. This seems counterintuitive since we would expect laser exposure to be an 'etching' process [30–32, 35], and therefore the membrane thickness would be reduced, if not remain the same. We hypothesized that this counterintuitive behavior is due to the fact that our experiment was performed in air of 0% humidity, rather than in salt solutions [30–32, 35]. The increase in thickness in our experiment is most likely due to the photo-oxidation of SiN_x by reaction with oxygen in the air [59]. Further material analysis would be required to test this hypothesis. This result, together with previous results of laser etching in salt solutions [30–32, 35], clearly demonstrated that the laser-SiN_x reactivity is a complex photochemical and photothermal process, where the surrounding environment (e.g. dry/wet, electrolyte concentration) would play a

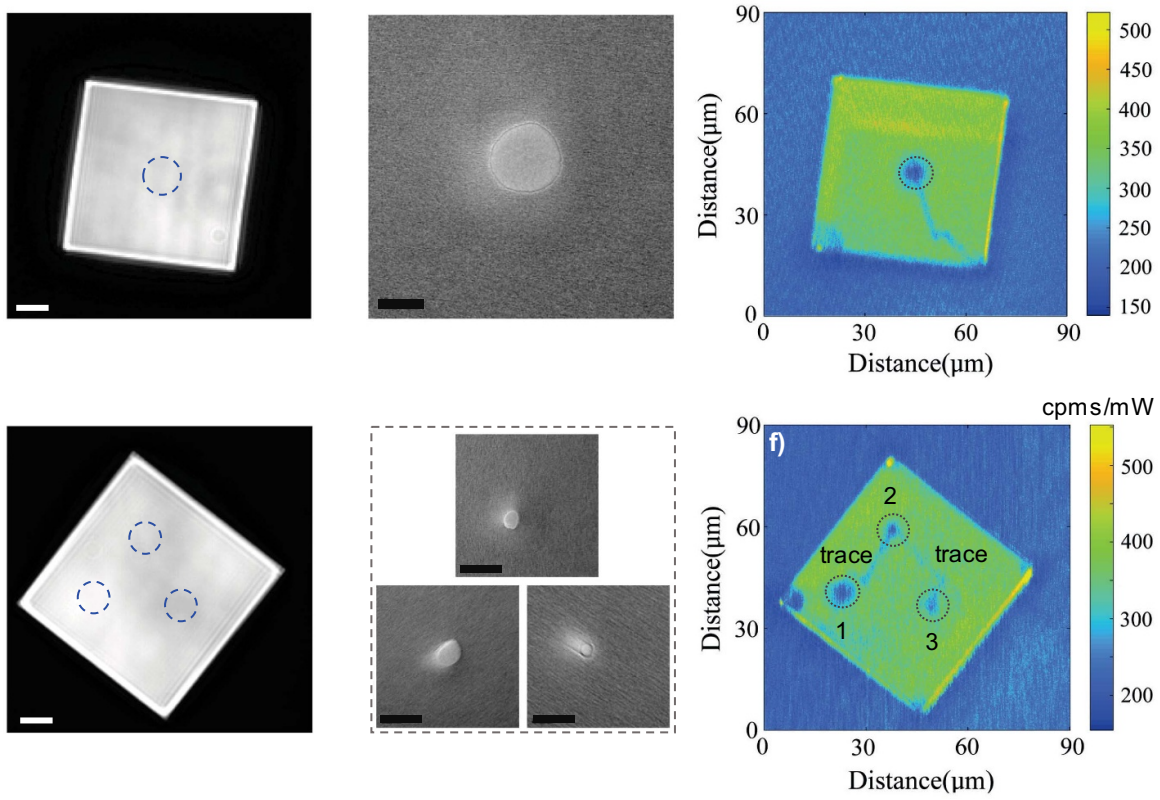

Figure 5. (a) Microscope image of an SiN_x membrane in which a single nanopore was drilled in the center, the e-beam was moved from the bottom right corner to the center of the membrane before drilling; scale bar, 10 μm. (b) Corresponding TEM image of the nanopore; scale bar, 20 nm. (c) The resulting PL map showing that a trace followed the e-beam path. (d) Microscope image with three nanopore locations annotated; the e-beam was successively moved to the next position after the preceding nanopore was created; scale bar, 10 μm. (e) Corresponding nanopores TEM images; scale bars, 20 nm. (f) The resulting PL map, which shows clear traces. PL scanning was performed at laser power 1 mW, integration time 2 ms and scanning step 300 nm.

significant role due to differing heat dissipation and chemical background.

Figure 6(d) quantifies the PL reduction as a function of laser exposure time for various laser powers in air. The PL intensity decreases linearly with the exposure time even when the laser power is small. This strongly suggests that great caution needs to be taken in producing and interpreting the PL map for SiN_x nanopore characterization. For example, probing the PL map around a nanopore at high laser power would itself change the intrinsic PL profile (supplementary figure S2). Figure 6(e) shows the percentage reduction in PL as a function of cumulative laser energy. We found that a cumulative laser energy less than 300 mJ would result in less than 3% of the PL reduction, while a cumulative laser energy larger than 5000 mJ would induce more than 10% of PL reduction (figure 6(e)). In most of our scanning PL measurements, 1 mW laser power and 2 ms integration time (total energy ~ 2 μJ) were used to minimize the impact of the probing laser on the material's intrinsic PL properties.

Lastly, as an interesting demonstration of laser-induced change in PL, we converted the letters 'PSU' into a binary image with 12 × 34 pixels. Each pixel represents a laser scan step of 1 μm (i.e. the letters were written into the 12 × 34 μm^2 area on the SiN_x membrane). All pixels with a binary value of '1' were exposed to a 20 mW, 488 nm laser for 10 s (i.e. total energy of 200 mJ, which is sufficient to cause PL reduction as shown in figure 6(e)). After this writing process, we examined the PL map under 1 mW laser power and 2 ms integration time. As shown in figure 6(f), the 'PSU' pattern is visible in the PL map, which confirms that the laser energy of 200 mJ indeed significantly changed the local microscopic properties of the material.

3. Conclusions

In summary, we demonstrated the use of confocal scanning PL for mapping microscopic changes in SiN_x nanopores exposed to electron and laser beams. We developed and validated a numerical model for the quantitative interpretation of the scanned PL result. We showed that the scanning PL result is independent of the nanopore size. The significant reduction in PL is contributed by the product of two microscopic material factors: quantum yield profile (i.e. variations in electronic structure) and thickness profile (i.e. thinning of the membrane). With this understanding, we experimentally demonstrated that unintentional electron and laser beam exposure would significantly change the electronic structures in the SiN_x membrane even when there is no visible thinning of the membrane. Our results unambiguously showed that it is critical to

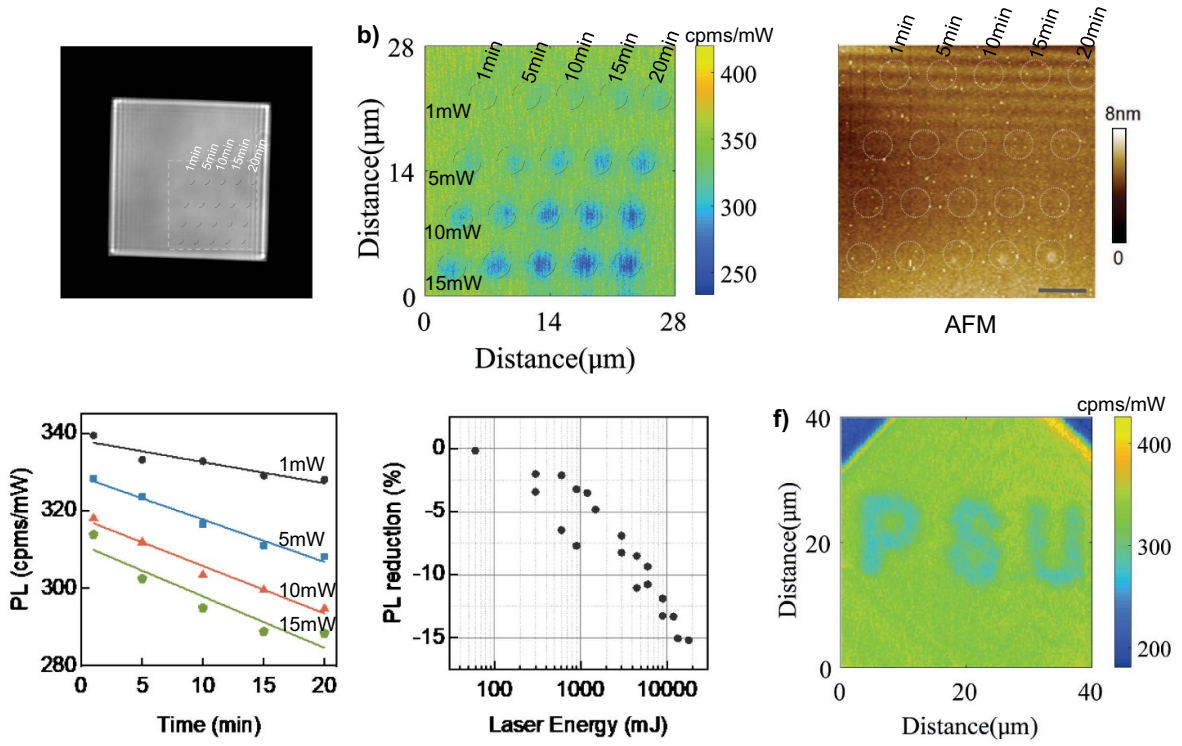

Figure 6. (a) Image of the SiN_x membrane showing the locations exposed to the focused 488 nm laser. (b) Resulting PL map after laser exposure (laser power 1 mW, integration time 2 ms, scanning step 100 nm). (c) AFM image from the same sample; the scale bar is 5 μm. The obvious change in morphology (increase in thickness) was observed at high laser powers. (d) PL reduction as a function of laser exposure time at various powers. Each data point was the average PL value of the area exposed to the laser (dashed circle in (b)). (e) Percentage reduction in PL as a function of cumulative laser energy. (f) PL map showing a laser-written pattern of letters 'PSU'.

minimize the unintended electron or laser beams to the SiN_x during the fabrication if one desires the microscopic integrity of the membrane. We anticipate this study can provide experimental insights into properly using and interpreting the scanned PL map to characterize beam-fabricated SiN_x nanopores.

4. Methods

4.1. Optical setup

The 488 nm Gaussian-profile laser (Coherent) was firstly expanded to completely fill the back aperture before focusing at the SiN_x membrane through the microscope objective lens (magnification 40×, numerical aperture 0.75) to form a diffraction-limited spot for confocal illumination. The radius of the laser spot is ~1.2 μm. The emitted light was collected by the same objective lens and focused on a pinhole of 25 μm diameter (National Aperture) for improved spatial resolution. The setup was also equipped with a CMOS camera (Thorlabs) for monitoring the positions of the membrane and laser spots. The emission light was filtered by a bandpass filter before being detected by the single-photon counting module (SPCM-AQRH-13). A neutral-density (ND) filter was mounted in the front of the photon counter to expand the dynamic range.

4.2. Scanning setup

The SiN_x nanopore chip was sealed on to a custom-built PMMA cell. The cell was mounted on a nanopositioner (Physik Instrumente, P-611.3 S NanoCube). The scanned PL map was obtained by a customized LabVIEW program (National Instruments) that controls the motion of the nanopositioner as well as acquiring the photon counting signals. Note that the spatial resolution is limited by the laser spot size and point spread function of the pinhole, which can be calculated from the HWHM of the CAF; too fine a scanning step would not necessarily increase the resolution (supplementary figure S3) and can lead to excessive laser energy being delivered to the membrane, which itself can impact the PL reduction. The typical parameters for obtaining the scanned PL results in our experiments are 100 nm step size, 1 mW laser power and 2 ms integration time. These parameters were used to ensure that the probing laser is non-destructive to the intrinsic properties of the sample under test. The PL results obtained in this study were from measurements in air unless otherwise noted.

4.3. TEM SiN_x nanopore fabrication

The 30 nm thick SiN_x membranes with 50 × 50 μm^2 window (NT005X) were purchased from Norcada. The nanopore was

drilled with a field-emission TEM (JEOL JEM-2100 F, operated at 200 kV). A medium magnification (120k) was first used to locate the window area before changing to high magnification (1000k) to tightly focus the electron beam onto the SiN_x membranes. Different nanopore sizes could be drilled by controlling the exposure time. TEM characterization of the nanopore was performed immediately after the drilling.

4.4. Numerical simulations

The model parameters (absorption coefficient, quantum yield, background count rate, dark count rate and system collection efficiency) were experimentally determined (figure 3 and supplementary table S1). With these parameters, equation (4) was numerically solved using a custom-built MATLAB code to obtain the scanned PL map.

Acknowledgments

This work was partially supported by the National Science Foundation under Grant No. 1710831. Any opinions, findings, and conclusions or recommendations expressed in this work are those of the authors and do not necessarily reflect the views of the National Science Foundation. WG acknowledges the support from Penn State Startup Fund. XH acknowledges the support from China Scholarship Council and National Natural Science Foundation of China (No. 61804071).

Associated content

Supporting Information is available, which contains detailed descriptions of the HWHM of the confocal acceptance function, decay of the laser-induced quantum yield, simulated PL maps at various scanning steps, and experimentally extracted model parameters.

Author contributions

XH performed the PL experiments and simulations, ZT performed the AFM experiments, SL and ML performed TEM nanopore fabrication. WG conceived the concept and supervised the study, WG and XH analyzed the data and co-wrote the manuscript.

Conflict of interest

The authors declare no competing financial inte Shasha rest.

ORCID iD

Weihua Guan https://orcid.org/0000-0002-8435-9672

References

[1] C, Henley R Y, Stoloff D H, Rynearson K D, Hermann T and Wanunu M 2014 Nanopore-based conformational analysis of a viral RNA drug target *ACS Nano* **8** 6425–30
[2] Nouri R, Jiang Y, Lian X L and Guan W 2020 Sequence-specific recognition of HIV-1 DNA with solid-state CRISPR-Cas12a-assisted nanopores (SCAN) *ACS Sensors* **5** 1273–80
[3] Tang Z, Choi G, Nouri R and Guan W 2019 Loop-mediated isothermal amplification-coupled glass nanopore counting toward sensitive and specific nucleic acid testing *Nano Lett.* **19** 7927–34
[4] Reza N, Tang Z and Guan W 2019 Calibration-free nanopore digital counting of single molecules *Anal. Chem.* **91** 10915–1488
[5] Japrung D, Dogan J, Freedman K J, Nadzeyka A, Bauerdick S, Albrecht T, Kim M J, Jemth P and Edel J B 2013 Single-molecule studies of intrinsically disordered proteins using solid-state nanopores *Anal. Chem.* **85** 2449–56
[6] Rosen C B, Rodriguez-Larrea D and Bayley H 2014 Single-molecule site-specific detection of protein phosphorylation with a nanopore *Nat. Biotechnol.* **32** 179–81
[7] Li J L, Gershow M, Stein D, Brandin E and Golovchenko J A 2003 DNA molecules and configurations in a solid-state nanopore microscope *Nat. Mater.* **2** 611–5
[8] Storm A J, Chen J H, Zandbergen H W and Dekker C 2005 Translocation of double-strand DNA through a silicon oxide nanopore *Phys. Rev.* E **71** 051903
[9] Venkatesan B M, Shah A B, Zuo J M and Bashir R 2010 DNA sensing using nanocrystalline surface-enhanced Al_2O_3 nanopore sensors *Adv. Funct. Mater.* **20** 1266–75
[10] Wang R, Gilboa T, Song J X, Huttner D, Grinstaff M W and Meller A 2018 Single-molecule discrimination of labeled DNAs and polypeptides using photoluminescent-free TiO_2 nanopores *ACS Nano* **12** 11648–56
[11] Larkin J, Henley R, Bell D C, Cohen-Karni T, Rosenstein J K and Wanunu M 2013 Slow DNA transport through nanopores in hafnium oxide membranes *ACS Nano* **7** 10121–8
[12] Merchant C A *et al* 2010 DNA translocation through graphene nanopores *Nano Lett.* **10** 2915–21
[13] Garaj S, Hubbard W, Reina A, Kong J, Branton D and Golovchenko J A 2010 Graphene as a subnanometre trans-electrode membrane *Nature* **467** 190–3
[14] Liu K, Feng J D, Kis A and Radenovic A 2014 Atomically thin molybdenum disulfide nanopores with high sensitivity for DNA translocation *ACS Nano* **8** 2504–11
[15] Waduge P, Bilgin I, Larkin J, Henley R Y, Goodfellow K, Graham A C, Bell D C, Vamivakas N, Kar S and Wanunu M 2015 Direct and scalable deposition of atomically thin low-noise MoS_2 membranes on apertures *ACS Nano* **9** 7352–9
[16] Shim J, Banerjee S, Qiu H, Smithe K K H, Estrada D, Bello J, Pop E, Schulten K and Bashir R 2017 Detection of methylation on dsDNA using nanopores in a MoS_2 membrane *Nanoscale* **9** 14836–45
[17] Thiruraman J P *et al* 2018 Angstrom-size defect creation and ionic transport through pores in single-layer MoS_2 *Nano Lett.* **18** 1651–9
[18] Liu S *et al* 2013 Boron nitride nanopores: highly sensitive DNA single-molecule detectors *Adv. Mater.* **25** 4549–54
[19] Park K B, Kim H J, Kim H M, Han S A, Lee K H, Kim S W and Kim K B 2016 Noise and sensitivity characteristics of solid-state nanopores with a boron nitride 2-D membrane on a pyrex substrate *Nanoscale* **8** 5755–63

[20] Danda G *et al* 2017 Monolayer WS_2 nanopores for DNA translocation with light-adjustable sizes *ACS Nano* **11** 1937–45

[21] Mojtabavi M, VahidMohammadi A, Liang W T, Beidaghi M and Wanunu M 2019 Single-molecule sensing using nanopores in two-dimensional transition metal carbide (MXxene) membranes *ACS Nano* **13** 3042–53

[22] Yemini M, Hadad B, Liebes Y, Goldner A and Ashkenasy N 2009 The controlled fabrication of nanopores by focused electron-beam-induced etching *Nanotechnology* **20** 245302

[23] Kim M J, McNally B, Murata K and Meller A 2007 Characteristics of solid-state nanometre pores fabricated using a transmission electron microscope *Nanotechnology* **18** 205302

[24] Prakash S, Pinti M and Bellman K 2012 Variable cross-section nanopores fabricated in silicon nitride membranes using a transmission electron microscope *J. Micromech. Microeng.* **22** 067002

[25] Chen C-H, Chang X and Wu C-S 2019 A novel shaped-controlled fabrication of nanopore and its applications in quantum electronics *Sci.Rep.* **9** 1–7

[26] Qian H and Egerton R F 2017 Solid-state nanopores of controlled geometry fabricated in a transmission electron microscope *Appl. Phys. Lett.* **111** 193106

[27] Li J, Stein D, McMullan C, Branton D, M J A and Golovchenko J A 2001 Ion-beam sculpting at nanometre length scales *Nature* **412** 166–9

[28] Chou Y-C, Masih Das P, Monos D S and Drndic M 2020 Lifetime and stability of silicon nitride nanopores and nanopore arrays for ionic measurements *ACS Nano* acsnano.9b09964

[29] Petrov Y V, Ubyivovk E and Baraban A 2019 Fabrication of nanopores in silicon nitride membrane by means of wet etching enhanced by focused helium ion beam irradiation AIP Conference Proceedings**2064** 030012

[30] Gilboa T, Zrehen A, Girsault A and Meller A 2018 Optically-monitored nanopore fabrication using a focused laser beam *Sci. Rep.* **8** 9765

[31] Gilboa T, Zvuloni E, Zrehen A, Squires A H and Meller A 2019 Automated, ultra-fast laser-drilling of nanometer scale pores and nanopore arrays in aqueous solutions *Adv. Funct. Mater.* **30** 1900642

[32] Yamazaki H, Hu R, Zhao Q and Wanunu M 2018 Photothermally assisted thinning of silicon nitride membranes for ultrathin asymmetric nanopores *ACS Nano* **12** 12472–81

[33] Kwok H, Briggs K and Tabard-Cossa V 2014 Nanopore fabrication by controlled dielectric breakdown *PLoS One* **9** 92880

[34] Roshan K A, Tang Z and Guan W 2019 High fidelity moving Z-score based controlled breakdown fabrication of solid-state nanopore *Nanotechnology* **30** 095502

[35] Ying C, Houghtaling J, Eggenberger O M, Guha A, Nirmalraj P, Awasthi S, Tian J and Mayer M 2018 Formation of single nanopores with diameters of 20–50 nm in silicon nitride membranes using laser-assisted controlled breakdown *ACS Nano* **12** 11458–70

[36] Deshpande S V, Gulari E, Brown S W and Rand S C 1995 Optical properties of silicon nitride films deposited by hot filament chemical vapor deposition *J. Appl. Phys.* **77** 6534–41

[37] Giorgis F, Vinegoni C and Pavesi L 2000 Optical absorption and photoluminescence properties of a-$Si_{1-x}N_x$:H films deposited by plasma-enhanced CVD *Phys. Rev.* B **61** 4693–8

[38] Park N-M, Choi C-J, Seong T-Y and Park S-J 2001 Quantum confinement in amorphous silicon quantum dots embedded in silicon nitride *Phys. Rev. Lett.* **86** 1355

[39] Wang M, Li D, Yuan Z, Yang D and Que D 2007 Photoluminescence of Si-rich silicon nitride: defect-related states and silicon nanoclusters *Appl. Phys. Lett.* **90** 131903

[40] Kistner J, Chen X, Weng Y, Strunk H, Schubert M and Werner J 2011 Photoluminescence from silicon nitride—no quantum effect *J. Appl. Phys.* **110** 023520

[41] Assad O N, Di Fiori N, Squires A H and Meller A 2014 Two color DNA barcode detection in photoluminescence suppressed silicon nitride nanopores *Nano Lett.* **15** 745–52

[42] Basché T, Ambrose W and Moerner W 1992 Optical spectra and kinetics of single impurity molecules in a polymer: spectral diffusion and persistent spectral hole burning *J. Opt. Soc. Am.* B **9** 829–36

[43] Moerner W and Fromm D P 2003 Methods of single-molecule fluorescence spectroscopy and microscopy *Rev. Sci. Instrum.* **74** 3597–619

[44] Moehl S, Zhao H, Don B D, Wachter S and Kalt H 2003 Solid immersion lens-enhanced nano-photoluminescence: principle and applications *J. Appl. Phys.* **93** 6265–72

[45] Liu B H, Dong Z L, Hua Y N, Fu C, Li X M, Tan P K and Zhao Y Z 2018 Electron-beam radiation induced degradation of silicon nitride and its impact to semiconductor failure analysis by TEM *AIP Adv.* **8** 115327

[46] Zhang P, Chen K, Lin Z, Tan D, Dong H, Li W, Xu J and Huang X 2016 Dynamics of high quantum efficiency photoluminescence from N-Si-O bonding states in oxygenated amorphous silicon nitride films *Appl. Phys. Lett.* **108** 111103

[47] Cosslett V 1978 Radiation damage in the high resolution electron microscopy of biological materials: a review *J. Microsc.* **113** 113–29

[48] Egerton R, Li P and Malac M 2004 Radiation damage in the TEM and SEM *Micron* **35** 399–409

[49] Howitt D, Chen S, Gierhart B, Smith R and Collins S 2008 The electron beam hole drilling of silicon nitride thin films *J. Appl. Phys.* **103** 024310

[50] Kato H, Kashio N, Ohki Y, Seol K S and Noma T 2003 Band-tail photoluminescence in hydrogenated amorphous silicon oxynitride and silicon nitride films *J. Appl. Phys.* **93** 239–44

[51] Ruggeri R, Neri F, Sciuto A, Privitera V, Spinella C and Mannino G 2012 Luminescence properties of SiO_xN_y irradiated by IR laser 808 nm: the role of Si quantum dots and Si chemical environment *Appl. Phys. Lett.* **100** 042104

[52] Jou S, Liaw I-C, Cheng Y-C and Li C-H 2013 Light emission of silicon oxynitride films prepared by reactive sputtering of silicon *J. Lumin.* **134** 853–7

[53] Mastronardi M L, Maier-Flaig F, Faulkner D, Henderson E J, Kübel C, Lemmer U and Ozin G A 2011 Size-dependent absolute quantum yields for size-separated colloidally-stable silicon nanocrystals *Nano Lett.* **12** 337–42

[54] Dal Negro L, Yi J, Michel J, Kimerling L, Chang T-W, Sukhovatkin V and Sargent E 2006 Light emission efficiency and dynamics in silicon-rich silicon nitride films *Appl. Phys. Lett.* **88** 233109

[55] Museur L, Zerr A and Kanaev A 2016 Photoluminescence and electronic transitions in cubic silicon nitride *Sci. Rep.* **6** 18523

[56] Tabard-Cossa V, Trivedi D, Wiggin M, Jetha N N and Marziali A 2007 Noise analysis and reduction in solid-state nanopores *Nanotechnology* **18** 305505

[57] Smeets R M M, Keyser U F, Dekker N H and Dekker C 2008 Noise in solid-state nanopores *Proc. Natl Acad. Sci. USA* **105** 417–21

[58] Liang S, Xiang F, Tang Z, Nouri R, He X, Dong M and Guan W 2020 Noise in nanopore sensors: sources, models, reduction, and benchmarking *Nanotechnol. Precis. Eng.* **3** 9–17

[59] Raider S I, Flitsch R, Aboaf J A and Pliskin W A 1976 Surface oxidation of silicon-nitride films *J. Electrochem. Soc.* **123** 560–5